Increased Coding Capacity of Chipless RFID Tags Using Radiation Pattern Diversity

Florian Requena, Nicolas Barbot, Darine Kaddour, Etienne Perret

Increased Coding Capacity of Chipless RFID Tags Using Radiation Pattern Diversity

Florian Requena[1], Nicolas Barbot[2], Darine Kaddour[3], Etienne Perret[4]
Univ. Grenoble Alpes, Grenoble INP, LCIS, F-26000 Valence, France
{[1]florian.requena, [2]nicolas.barbot, [3]darine.kaddour, [4]etienne.perret}@lcis.grenoble-inp.fr

***Abstract* — In this paper, a method to increase the coding capacity of chipless RFID tags is proposed. This approach is based on the radiation pattern diversity of different resonators topology or different modes of resonance on the same resonator topology. By using two antennas and therefore two mono-static measurements, with these tags, it is possible to double the coding capacity without increasing the frequency band of operation. In the present manuscript, conventional chipless RFID loop resonators are considered. Two modes of resonance will be exhibited for this resonator and used to encode data. The novelty is the usage of the same frequency slot to encode multiple bits without interfering together.**

***Keywords* — Coding capacity, Chipless RFID, Radar, Reading method, Scatterer.**

I. Introduction

RFID (Radio Frequency IDentification) is an identification technique that uses backscatterer modulation principle to identify tags in applications similar to barcodes. Chipless RFID is one competitive technology which consists in removing the electrical component of conventional RFID tags to reduce the tag cost. This technology has seen a significant increase in recent years, both in terms of applications and research efforts. Reading robustness, sensing applications, or inkjet printing techniques are among the works available. Research efforts have also been put in the coding capacity of such tags. Chipless RFID data can be encoded on the electromagnetic backscattering wave of the tag by different phenomena : delays for time domain, frequency of resonance in the frequency domain, spatial distribution of resonators for imaging approaches,... A recent comparison of the data encoding of such approaches is presented in [1] and is summarized in Table. 1. The proposed method is based on the spatial diversity which can be compared to imaging technique similar to [2] in that it allows a tag to be made with several resonators having the same resonance frequency. However the approach introduced is not based on imaging. The novelty is the use of harmonics and radiation patterns to achieve this new reading method.

Frequency coded chipless tags are composed of several resonators such as illustrated in Fig. 1. When an incoming electromagnetic wave illuminates a tag, resonators will back-scatter some energy at their resonance frequencies. Since each resonator has its own resonance frequency (the frequency where the resonator dimension is $\lambda/2$ - see Fig. 1), it is possible to differentiate each resonator individually. Based on this principle, diverse data encoding schemes have been proposed. A conventional encoding scheme is the On-Off Keying modulation : a frequency band will be chosen and divided into sub-frequency slots. Each frequency slot is associated to a bit of data. If a resonance peak is present in a frequency slot, the bit is set to '1'. If no peak is present, the bit is set to '0'. The simplicity and robustness of this encoding scheme explains its widespread. In this paper, a method to encode multiple resonance peaks into a single frequency slot will be presented to increase the coding capacity for a constant total frequency range. This propriety is comparable to polarization method [3] but this approach can increase the coding capacity with the number of harmonics used to encode date. We show that an approach based on diversity of reading also allows to consider an increase in coding using this principle.

Table 1. Comparison of coding capacity in chipless RFID [1].

Technique	Type of tag	bit/cm^2
Time domain	SAW [4]	<1
	TDR [5]	0.17
Frequency domain	Slot [6]	<4.2
	Spiral [7]	0.61
	C-shape [8]	1.14
Hybrid	Frequency-phase [9]	2.86
	Frequency-angle [10]	0.52
	Frequency-Magnitude [1]	3
Spatial-domain	SAR [2]	2
	INSAR, SAR [11]	1.6
Polarization	Split ring [3]	3

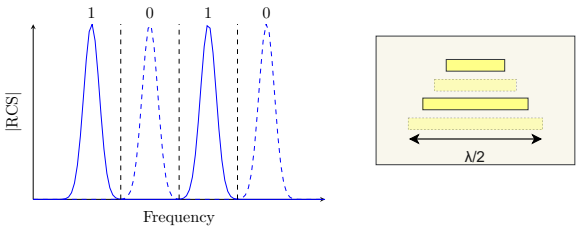

Fig. 1. a) Illustration of a chipless RFID tags using On-Off-Keying encoding.

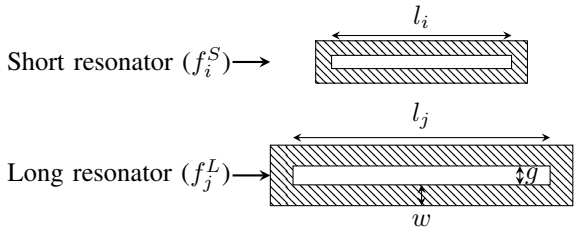

Fig. 2. Schematic of the long and short loop resonators used in this study.

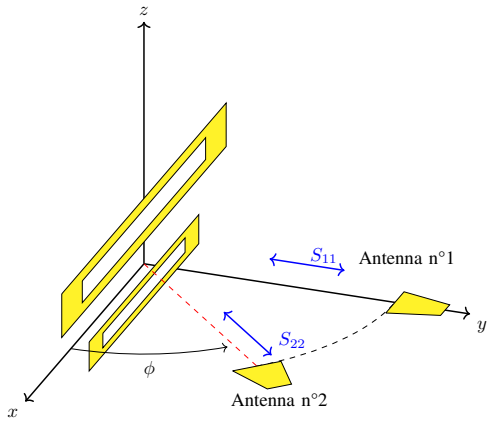

Fig. 3. Loop scatterers, coordinate system and notations considered in this paper. Antenna n°1 is aligned with the y-axis while antenna n°2 is oriented along the ϕ angle.

Fig. 4. Equivalent model of the loop resonator. The loop is replaced by two small dipoles spaced $\lambda/2$ apart with λ taken at the fundamental resonance frequency of the loop f_1.

II. Principle

Rectangular loops are considered in this study (see Fig. 2). Fig. 3 presents the measurement setup principle. The coordinate system used in this paper is given in Fig. 3. The loops are positioned in the xOz plane centered around the origin of the coordinate system. The antenna n°1 is positioned at normal incidence to the tags. The angle ϕ is between the loops and the antenna n°2.

When impinged by a plane wave along the y direction, significant currents are induced along the small arms of the loop at the fundamental frequency and the harmonics. These currents are in phase at the fundamental frequency and for odd harmonics while they are in opposition of phase for even harmonics. As a result, we can model the loop resonator as two small dipoles of length L and spaced $\lambda/2$ apart in the z direction as illustrated in Fig. 4 with λ taken at the fundamental frequency f_1. If we consider two dipoles with the same current I_0, the total radiated electric field $\vec{E_s}$ can be obtained using the array-factor (AF) from the array-antenna theory knowing the electric field radiated by a single infinitesimal dipole $\vec{E_d}$. At the fundamental frequency, the total amplitude of the radiating field $E_s(f_1)$ at $\theta = 90°$ is given by [12] :

$$E_s(f_1) = E_d \times AF_1 = k_1 \frac{\eta I_1 L}{16\pi r} \left[\frac{\sin(\pi \cos(\phi))}{\sin\left(\frac{\pi}{2}\cos(\phi)\right)} \right]^2 \quad (1)$$

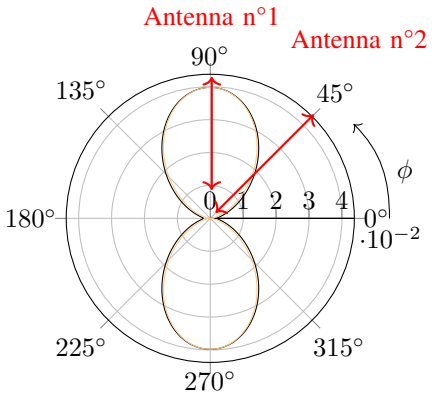

(a)

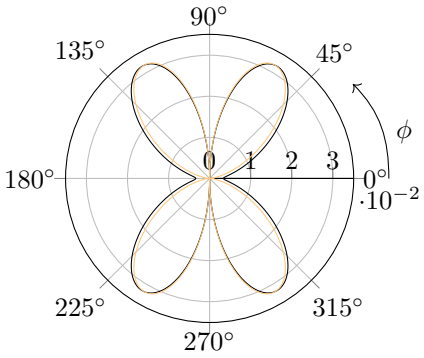

(b)

Fig. 5. Magnitude of the E-field (V/m) radiated by the loop for $\phi \in [0°; 360°]$ at (a) the fundamental frequency and (b) the first harmonic. In black the CST simulation and in yellow the expressions obtained from [12].

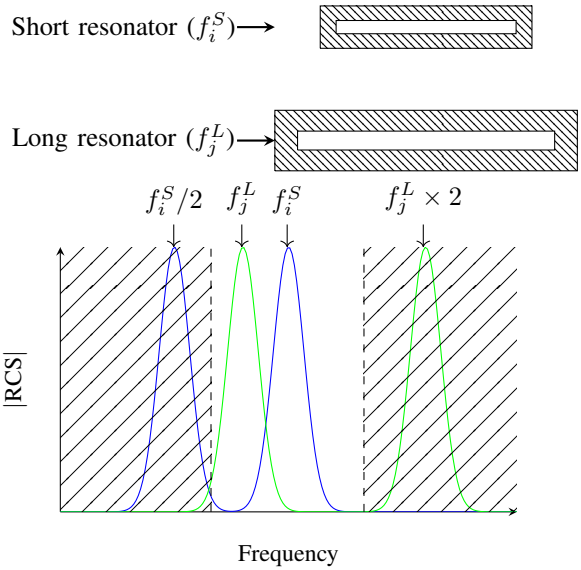

Fig. 6. Frequency band considered where some resonators work at their fundamental frequencies f_j^L and some work at their first harmonic f_i^S. The hatched areas are not used to encode information.

where k is the wave number, r the distance from the resonator to the antenna and η the impedance of free space.

Using the same procedure, the first harmonic at $\theta = 90°$ can be written as [12] :

$$\begin{aligned} E_s(f_2) &= E_d \times AF_2 \\ &= k_2 \frac{\eta I_2 L}{16\pi r} \sin(\theta) \left[\frac{\sin(2\pi \cos(\phi) + \pi)}{\sin\left(\pi \cos(\phi) + \frac{\pi}{2}\right)} \right]^2 \\ &= 2k_2 \frac{\eta I_2 L}{16\pi r} \sin(\theta) \Big[\sin\left(\pi \cos(\phi)\right) \Big]^2 \end{aligned} \tag{2}$$

The expressions of the radiated fields are compared with the ones retrieved from a CST MW simulation in Fig. 5 for the fundamental frequency and the first harmonic. Values of I_1 and I_2 has been normalized to the simulation amplitude. We can see that the analytical model and the simulation are in good agreement for the whole radiation pattern as well as the harmonic.

We can also notice that with this resonator more data can be encoded using blind spots of the radiation pattern if harmonics are used. Indeed, if we place an antenna at $\phi = 90°$, long loop resonators working at their fundamental frequencies (f_i^L) can be seen according to their radiation patterns (see Fig. 5a) but short loop resonators working at their first harmonic (f_i^S) can not be seen (see Fig. 5b). Now, if a second antenna is placed at $\phi \neq 90°$, both resonators can be seen according to their radiation patterns. An illustration of the requested frequency band is presented in Fig. 6. Note that first resonance (for small loop) and second resonance (for long loop) can lie outside the operating frequency band of the reader. These peaks do not impact the proposed method since chipless tags are linear time-invariant systems. The protocol to read both modes of resonance (even at the same resonance frequency $f_i^S = f_j^L$), is based on two measurement with 2 antennas (see Fig. 3) is as follows : First, a S_{11} measurement at $\phi = 90°$ has to be done with antenna n°1. This measurement gives the response of loop resonators working at their fundamental frequencies only. Then, a S_{22} measurement needs to be done with antenna n°2 at the angle ϕ (see Fig. 3). Since the response of resonators operating at their fundamental frequency are known (using S_{11}), it is possible to remove their contributions from S_{22} to only have the resonators response operating at their first harmonic. Indeed, using (1) and (2), we know how much the contribution of resonators working at their fundamental is reduced at an angle ϕ.

In conclusion, resonance frequencies of resonators working at their fundamental frequency M^L can be obtained using :

$$M^L = S_{11} \tag{3}$$

For resonators operating at the first harmonic, the frequencies can be obtained from the following M^s signal :

$$M^S = S_{22} - S_{11} \times \sin\left(\frac{\pi}{2} \cos\phi\right)^2 \tag{4}$$

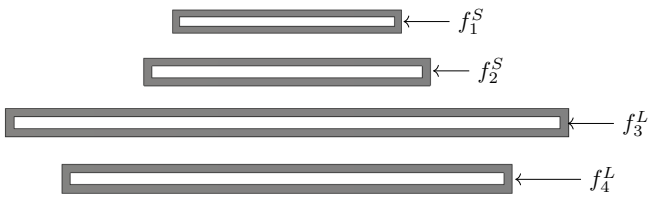

Fig. 7. Configuration of 4 loop resonators used for the simulation. The loops have the same g = 2mm and w = 1.4mm. Lengths are l_1 = 42.2mm, l_2 = 47.97mm, l_3 = 87mm and l_4 = 77mm.

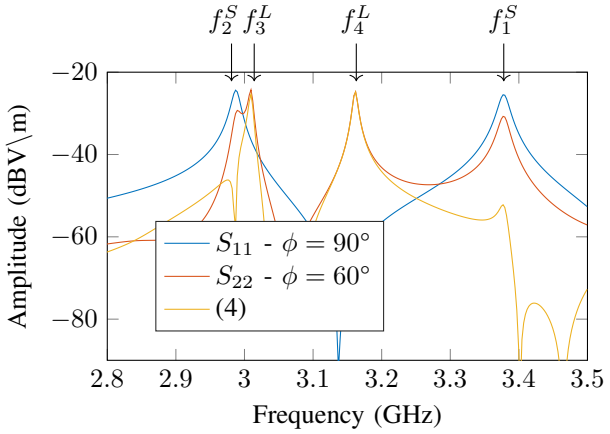

Fig. 8. Simulated E-fields response corresponding to S_{11} and S_{22} parameters for the 4 loop resonators illustrated in Fig. 7.

Using a configuration with two antennas and the first two modes of resonance it is possible to realize the reading of the short resonator and the long resonator independently. This procedure actually double the coding capacity since it is now possible to encode 2 bits per frequency slot (one relating to loops operating in their fundamental resonance frequency and one to loops operating in their first harmonic).

III. Simulations

Simulations have been carried out using CST MW to validate the approach. Four loop resonators, as illustrated in Fig. 7, were designed such as 2 of them operates at their fundamental mode of resonance while 2 others work at their first harmonic mode of resonance between 3GHz and 3.4GHz. Furthermore, one resonator at the fundamental frequency and one at the first harmonic have been chosen to share the same resonance frequency (frequency slot) at 3GHz. Simulated E-fields corresponding to S_{11} and S_{22} parameters are plotted in Fig. 8 for a second antenna placed at $\phi = 60°$. We can see on Fig. 8 that for S_{11}, only the two resonators working at their fundamental frequency are visible. Now with an angle of $\phi = 60°$ (S_{22}), we can notice that both modes of resonances are present. Using (4), we can successfully remove the fundamental response of resonators from S_{22}, leaving only the first harmonic mode. By doing so, one can encode data using the fundamental and harmonics on the same frequency slots.

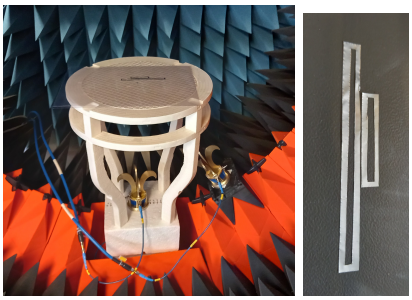

Fig. 9. a) Test bench inside the semi-anechoic chamber StarLab from MGV. b) The loop resonators used for the measurement. The first resonator has $g = 2$ mm, $w = 1.4$ mm and $l_1 = 47.97$ mm. The second resonator has the same g and w but $l_2 = 97$ mm.

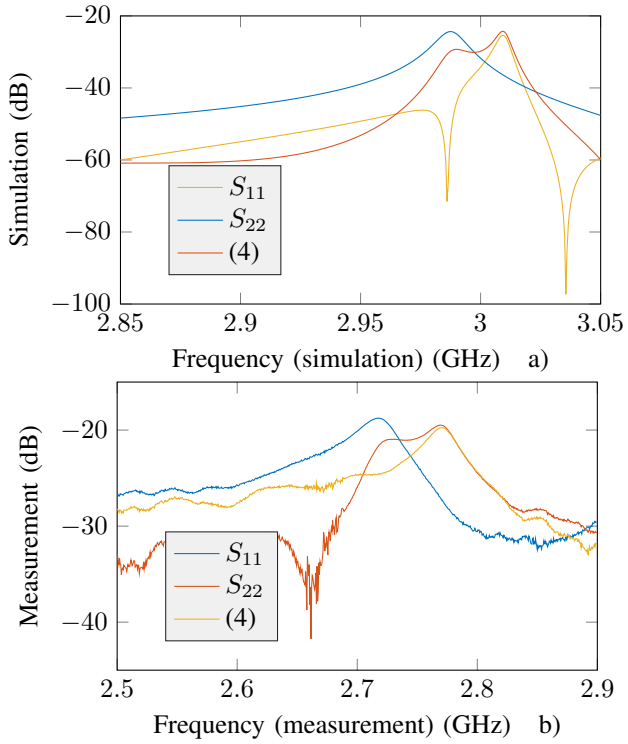

Fig. 10. S-parameters measured for the loop resonators shown in Fig. 9 in a) simulations and b) measurements.

IV. Measurements

Measurements in a semi-anechoic chamber inside a StarLab from MGV were achieved as shown in Fig. 9. A configuration with two antennas is used where antenna n°1 is placed at $\phi = 90°$ and antenna n°2 placed at $\phi = 60°$. The two resonators working at 3 GHz (on their fundamental and first harmonic) on the same frequency slot (dimensions are obtained from the simulation) have been cut in an aluminium sheet as shown in Fig. 9. S-parameters have been measured and (4) has been applied as plotted in Fig. 10. We can see that (4) allows to make the distinction between the two loops having the same resonance frequency. This results shows the potential of this new approach to increase the coding capacity by a factor 2.

V. Conclusion

In this paper, a method to increase the coding capacity with a constant frequency bandwidth of chipless tag was proposed. This approach is based on the radiation pattern diversity of same resonator topology but different mode of resonance. Simulations and measurements have shown the increase in the coding capacity using conventional loop resonators by different bits in a single frequency slot. We note that it is also possible to use the same principle with two different families of resonators, for example by mixing loops with C shape resonators. In this case the increase of the tag surface can be reduced. The increase in coding capacity imposes certain limitations, particularly in the positioning of the tags in relation to the reader. This type of approach can be implemented when the position of the tag is controlled, for example when the tagged objects are positioned on a rolling cart.

Acknowledgment

This project has received funding from the European Research Council (ERC) under the European Union's Horizon 2020 research and innovation program (grant agreement No 772539). This work is also supported by Univ. Grenoble Alpes.

References

[1] O. Rance, R. Siragusa, P. Lemaitre-Auger, and E. Perret, "Toward RCS magnitude level coding for chipless RFID," *IEEE Transactions on Microwave Theory and Techniques*, vol. 64, no. 7, pp. 2315–2325, 2016.

[2] M. Zomorrodi and N. C. Karmakar, "Cross-RCS based, high data capacity, chipless RFID system," in *2014 IEEE MTT-S International Microwave Symposium (IMS2014)*. IEEE, 2014, pp. 1–4.

[3] A. Vena, E. Perret, and S. Tedjini, "A compact chipless rfid tag using polarization diversity for encoding and sensing," in *2012 IEEE International Conference on RFID (RFID)*. IEEE, 2012, pp. 191–197.

[4] C. S. Hartmann, "A global SAW ID tag with large data capacity," in *2002 IEEE Ultrasonics Symposium, 2002. Proceedings.*, vol. 1. IEEE, 2002, pp. 65–69.

[5] B. Shao, Q. Chen, Y. Amin, S. M. David, R. Liu, and L.-R. Zheng, "An ultra-low-cost RFID tag with 1.67 gbps data rate by ink-jet printing on paper substrate," in *2010 IEEE Asian Solid-State Circuits Conference*. IEEE, 2010, pp. 1–4.

[6] A. El-Awamry, M. Khaliel, A. Fawky, M. El-Hadidy, and T. Kaiser, "Novel notch modulation algorithm for enhancing the chipless RFID tags coding capacity," in *2015 IEEE International Conference on RFID (RFID)*. IEEE, 2015, pp. 25–31.

[7] E. Perret, *Radio frequency identification and sensors: from RFID to chipless RFID*. John Wiley & Sons, 2014.

[8] A. Vena, E. Perret, and S. Tedjini, "A fully printable chipless RFID tag with detuning correction technique," *IEEE Microwave and Wireless Components Letters*, vol. 22, no. 4, pp. 209–211, 2012.

[9] A. Vena, E. Perret, and S. Tedjini, "Chipless RFID tag using hybrid coding technique," *IEEE Transactions on Microwave Theory and Techniques*, vol. 59, no. 12, pp. 3356–3364, 2011.

[10] C. Feng, W. Zhang, L. Li, L. Han, X. Chen, and R. Ma, "Angle-based chipless RFID tag with high capacity and insensitivity to polarization," *IEEE Transactions on Antennas and Propagation*, vol. 63, no. 4, pp. 1789–1797, 2015.

[11] S. Kofman, Y. Meerfeld, M. Sandler, S. Dukler, and V. Alchanatis, "Radio frequency identification system and data reading method," May 1 2012, uS Patent 8,167,212.

[12] F. Requena, N. Barbot, D. Kaddour, and E. Perret, "Modelling of the radiation pattern of a loop resonator for orientation sensing," *in review to IEEE Transactions on Antennas and Propagation*.